JOURNAL OF Materials CHEMISTRY

Quartz-crystal microbalance and spectrophotometric assessments of inter-core and inter-shell reactivities in nanoparticle thin film formation and growth

Li Han, Mathew M. Maye, Frank L. Leibowitz, Nam K. Ly and Chuan-Jian Zhong*

Department of Chemistry, State University of New York at Binghamton, Binghamton, New York, 13902, USA. E-mail: cjzhong@binghamton.edu

Received 16th August 2000, Accepted 30th January 2001
First published as an Advance Article on the web 5th March 2001

Spontaneous core–shell and shell–shell reactivities of thiolate-capped nanoparticles are exploited for assembling nanoparticle network thin films *via* an exchange–crosslinking–precipitation route. Gold nanoparticles of two different core sizes (2 and 5 nm) capped with decanethiolates and alkylthiols of two different functionalities, 1,9-nonanedithiol (NDT) and 11-mercaptoundecanoic acids (MUA), were studied as the assembly components. The film formation and growth involve inter-core covalent Au–thiolate bonding at both ends of NDT, or inter-shell non-covalent hydrogen-bonding at carboxylic acid terminals of MUA shells. The present work focuses on a kinetic assessment of the controlling factors based on UV-Visible spectrophotometric and quartz-crystal microbalance measurements. These measurements probe the evolution of the surface plasmon resonance band of nanoparticles and monitor the mass loading of the assembled films, respectively. Both qualitative and quantitative insights have been obtained for understanding the dependences of exchange, nucleation and crystallization processes on core size and shell structure. The implication of the results for designing nanostructured assemblies using core–shell nanoparticles as building blocks is discussed in terms of binding site, core size and shell structure.

Introduction

In comparison with conventional colloids or nanoparticles synthesized by reverse micelle, polymer encapsulation and vapor-phase production, organic monolayer (alkanethiolate)-capped gold, silver and alloy nanoparticles possess several unique attributes, including air stability, reversible solubility in common organic solvents and molecule-like reactivity.[1,2] Such nanoparticles consist of a metallic nanocrystal core within an organic monolayer shell. The core–shell attributes have been exploited in solution reactivities of organized and highly-dispersed nanoparticles,[3,4] and for generating nanostructured assemblies based on casting,[5] stepwise layer-by-layer construction[6–8] and DNA-based linking.[9] While there are growing interests in potential applications of the nanostructured materials in microelectronics, optic devices, magnetic materials, molecular recognition and catalysis,[1,10] a key area of research is the development of techniques in the nanoconstruction of functional nanomaterials.

As a simple and versatile means, we have recently demonstrated a new nanoconstruction route for self-assembling core–shell nanoparticles into thin films on substrates of almost any type.[11,12] This route, termed as one-step exchange–crosslinking–precipitation, exploits the spontaneous core–shell or shell–shell reactivities such as Au–dithiolate–Au covalent bonding[11] and hydrogen-bonding at carboxylic acid terminals.[12] These two general types of reactivities are depicted in Scheme 1 in a highly idealized fashion. In these reactions, an initial exchange reaction of free thiols with Au-bound thiolates in a solution is followed by either crosslinking reactions *via* inter-core Au–S bonding (upper route) or inter-shell carboxylic acid hydrogen bonding (lower route). Recent demonstrations of place-exchange[3] and shell derivatization[10] reactions to fabricate various shell functionalities serve as the starting point of our approach. Our approach further explores the follow-up crosslinking reactivities that eventually lead to deposition of the nanoparticles as thin film assemblies. The films thus formed are air-stable, and importantly, exhibit interesting electrochemical barrier and biomimetic nanochannel properties depending on the nanocrystal core sizes and the molecular shell networking properties.[11,12]

Although structures of the inter-core linkage and inter-shell head-to-head hydrogen bonding in these films were recently characterized using surface infrared reflection spectroscopy (IRS),[11,12] factors governing the film growth processes and controlling parameters have not been fully assessed. Such an assessment requires a clear understanding of chemical reactivities of nanoparticle encapsulation and solution components at inter-core or inter-shell binding sites. In this paper, we report the findings of a kinetic assessment of these reactivities based on UV-Visible spectrophotometric (UV-Vis) and quartz-crystal microbalance (QCM) measurements. These two types of measurement probe the evolution of the surface plasmon (SP) resonance band of the nanoparticles and monitor the thin film mass loading, respectively. The results have provided both qualitative and quantitative insights into the dependences of exchange, nucleation and crystallization processes on core size and shell structure. Specific issues include how the film growth is controlled by parameters such as immersion time and concentrations of the capped particles and the linking molecules, and what mechanistic factors are operative in the inter-core and the inter-shell molecular reactivities. Such insights should permit a better exploitation of the interfacial reactivities as a general route for assembling novel nanostructured materials for molecular recognition and catalysis.

Experimental

Chemicals

The chemicals used included decanethiol (DT, 96%), 11-mercaptoundecanoic acid (MUA, 97%), 1,9-nonanedithiol

 DOI: 10.1039/b006687g

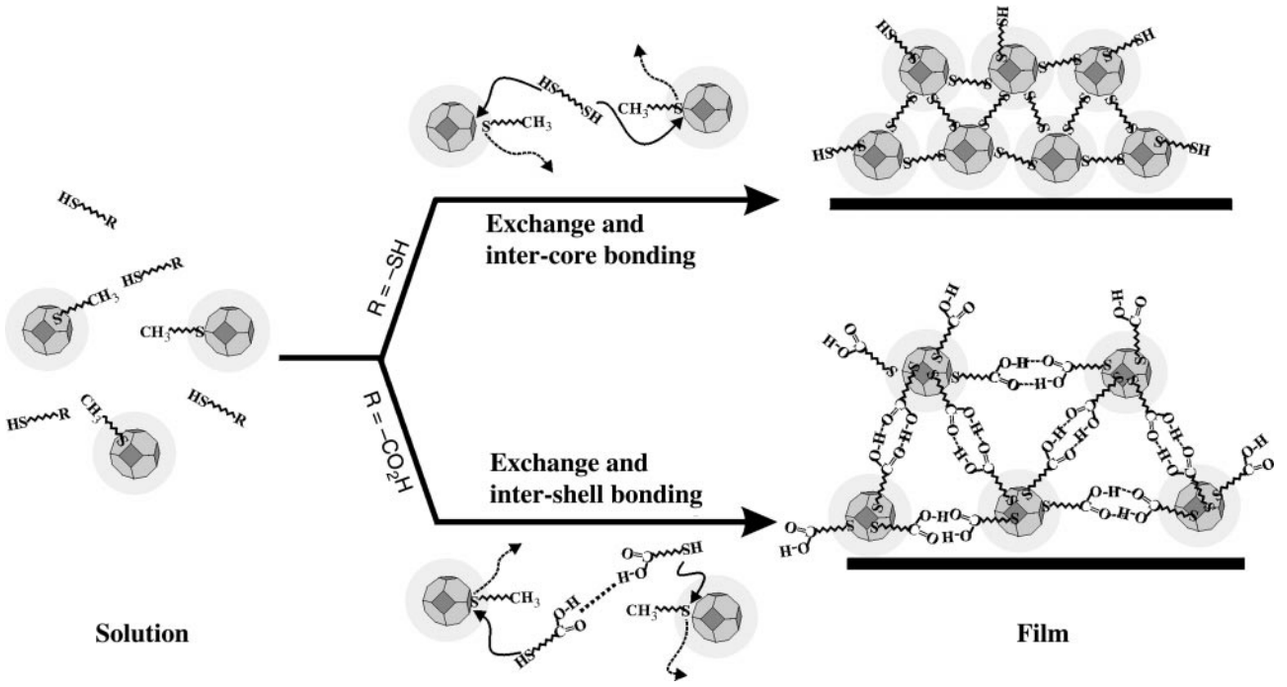

Scheme 1 Schematic illustrations of two types of interparticle molecular reactivities leading to the formation of nanoparticle thin films.

(NDT, 95%), hydrogen tetracholoroaurate ($HAuCl_4$, 99%), tetraoctylammonium bromide (TOABr, 99%), sodium borohydride ($NaBH_4$, 99%). Solvents included toluene (99.8%), hexane (99.9%), and ethanol (99.9%). All chemicals were purchased from Aldrich and used as received. Water was purified with a Millipore Milli-Q water system.

Nanoparticle preparation

Thiolate-capped gold nanoparticles of both 2 nm ($Au_{2\ nm}$) and 5 nm ($Au_{5\ nm}$) core sizes were prepared in this work. The $Au_{2\ nm}$ particles were synthesized by the standard two-phase method.[13] Briefly, $AuCl_4^-$ was first transferred from aqueous $HAuCl_4$ solution (10 mM) to toluene by the phase transfer reagent TOABr (36 mM). DT was then added at a 2 : 1 mole ratio of DT to Au. An excess (12 ×) of aqueous $NaBH_4$ was slowly added into the solution. The reaction was allowed to occur under stirring at room temperature for 4 h, producing a dark-brown solution of the DT-capped $Au_{2\ nm}$ (core size: 1.9 ± 0.7 nm). The solution was subjected to solvent removal in a rotary evaporator at room temperature and followed by multiple cleanings using ethanol.

$Au_{5\ nm}$ particles were derived from the $Au_{2\ nm}$ particles by a thermally-activated processing route, details of which were recently described.[14] Briefly, a solution of the $Au_{2\ nm}$ particles resulting from the synthesis was pre-concentrated before subsequent heating to a temperature of 140 °C, at which the core–shell structure undergoes desorption/re-deposition and coalescence/growth, and eventually evolves in core size.[14] The products, $Au_{5\ nm}$ (core size: 5.2 ± 0.3 nm), were subjected to subsequent suspension in ethanol at least three times to ensure complete removal of solvent and by-products. The core sizes of the nanoparticles were determined by transmission electron microscopy.[14]

Film preparation

Thin film assemblies of gold nanoparticles (Au_{nm}) were derived from MUA or NDT molecular linkages, which are denoted as MUA–Au_{nm} and NDT–Au_{nm} films, respectively. The general preparation involved immersion of substrates, glass or gold film on glass, into a solution of nanoparticles and crosslinking agents at room temperature. At different immersion times, the film-deposited substrates were emersed and rinsed thoroughly with solvent. Two preparation procedures were adopted that allowed monitoring of the film growth as a function of immersion time. One involved the use of different substrates to immerse for different time lengths; the other used the same substrate to immerse and re-immerse into the solution. No differences in terms of the trend of the kinetic data were observed between the two preparation methods, though there were about $\pm 10\%$ variations in absolute values of absorbance or frequency change data. Most of the data reported were collected using the single substrate unless otherwise noted. The substrates were immersed vertically in the solution to ensure the film was free of powders. The vessel was sealed from solvent evaporation after the substrate immersion. Thin film samples were rinsed with hexane and dried under nitrogen before characterization.

For preparing MUA–Au_{nm} films, stock solutions of DT-capped $Au_{5\ nm}$ (~ 5 μM) or $Au_{2\ nm}$ (~ 100 μM) in hexane (sometimes in toluene) and MUA (5.0 mM) in ethanol were used to prepare solutions. The concentration of nanoparticles is expressed in terms of the concentration of total particles in the solution calculated using the average particle core sizes. MUA was mixed with Au_{nm} in a hexane solvent at controlled concentrations, typically in the concentration ranges of 0.1–2.0 μM for $Au_{5\ nm}$, 1.0–10.0 μM for $Au_{2\ nm}$, and 0.05–5.0 mM for MUA. Typical MUA to nanoparticle ratios were in the range of 50–400 to 1. For NDT–Au_{nm} films, a similar procedure was used for the preparation. The DT-capped $Au_{5\ nm}$ or $Au_{2\ nm}$ particles and NDT dithiols were mixed in hexane. The concentration ranges were 0.5–2.0 μM for $Au_{5\ nm}$, 1–100 μM for $Au_{2\ nm}$, and 10–200 mM for NDT. Typical NDT to particle ratios were in the range of 1000–15000 to 1. Specific concentrations and ratios are indicated in the descriptions.

Substrates used for the thin film preparation included glass slides and gold film coated QCM devices. The glass slides were cleaned by sonicating in Micro-90 (Cole-Palmer) solution for 1 h, and rinsing with deionized water. The gold surfaces were cleaned by immersion in 1 : 3 H_2O_2 (30%)–H_2SO_4 (conc.) solution for 3 min, and rinsed with deionized water and ethanol (**Caution**: H_2O_2–H_2SO_4 solution reacts violently with organic compounds and should be handled with extreme care).

Instrumentation and measurements

UV-Vis spectra were acquired with a HP 8453 spectrophotometer. The optical band measured is characteristic of the surface plasmon resonance band of the nanoparticles. Nanoparticle thin film samples were deposited on glass slides (cover glass), and solution samples were prepared using hexane as solvent. Both were measured in transmission mode.

QCM measurements were performed on a custom-built oscillation circuitry with sine wave output (oscillator chip model MC12061L, Newark Electronics). The oscillator can operate in the frequency range 2–20 MHz. A HP frequency counter (Model 5302A) was used to measure frequency. AT-cut quartz crystals (cerium-polished on both sides with 1.3 cm diameter and 19 μm thickness, P.R. Hoffman Materials) with a 9 MHz fundamental resonance frequency were used. Gold films of 200 nm thickness were deposited onto both sides of the quartz disks in a "keyhole" shape. The quartz disks were primed with 15 nm of chromium prior to gold deposition. The gold film had an excitation electrode diameter of 0.45 cm with a geometric area of 0.63 cm^2. The device was housed in a stainless cap, and was purged with Ar for 5 min before each measurement. The resonance frequency was determined prior to and after the film deposition. The frequency change provides the measure of mass loading.

Results

The structures and morphologies of both MUA–Au_{nm} and NDT–Au_{nm} films have been characterized using infrared reflection spectroscopy and transmission electron microscopy, as detailed in recent reports.[11,12] This section describes the results of the UV-Vis and QCM measurements.

1. UV-Vis spectrophotometric measurement

In general, the SP resonance band for both MUA–$Au_{5\ nm}$ and NDT–$Au_{5\ nm}$ films appears at ~590 nm in the UV-Vis spectrum, which shows a small shift in wavelength and broadening in bandwidth in comparison with its solution counterpart (520 nm).[11,12] Thin films of MUA–$Au_{2\ nm}$ or NDT–$Au_{2\ nm}$ display a weak band superimposed on a rising spectral background, resembling its solution counterpart.[11,12] Since the $Au_{2\ nm}$ films do not show a distinctive band well resolved from its rising background, the spectral evolution data described next are mostly for the $Au_{5\ nm}$ systems.

Fig. 1 shows a set of UV-Vis spectra of NDT–$Au_{5\ nm}$ thin films deposited on a single glass substrate at different immersion times from a hexane solution of 20 mM NDT and 1.3 μM $Au_{5\ nm}$. The spectrum (dashed curve) of the particles in a hexane solution is included for comparison. The time interval between emersion and re-immersion, *i.e.*, the time spent for the optical measurement, was about 2–5 min. The spectra show two major features. First, the SP band displays a red shift (~70 nm) in comparison with the solution counterpart. As the film grows, it is slightly shifted to a longer wavelength (580–600 nm) than the solution counterpart (520 nm). The bandwidth is also shown to be greater for the film than for the solution. These subtle changes can be qualitatively related to a reduction in inter-core distance and in effective medium effect.[15] The bandwidth broadening relates to a range of interband transitions due to a range of interparticle distance distribution for the closely-spaced particles in the film in comparison with that in the solution counterpart. The overall spectral similarity between the film and the solution counterpart is indicative of an effective isolation of the particles by the NDT linkers that are shorter in length than the particle size.[9] A quantitative correlation of the shift and broadening with interparticle distance and effective medium property is however beyond the scope of the present work. Secondly, the intensity of

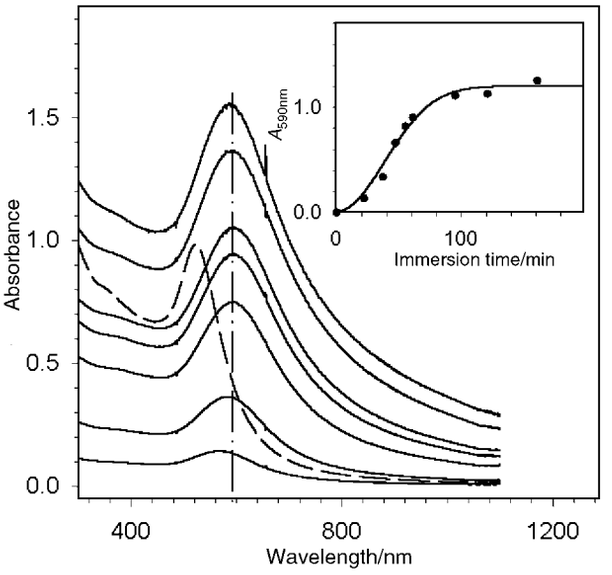

Fig. 1 UV-Vis spectra as a function of immersion time for the formation of a NDT–$Au_{5\ nm}$ film from a hexane solution containing 1.3 μM $Au_{5\ nm}$ and 20.0 mM NDT. Immersion time (min) increases from the bottom to the top. The immersion times are (from bottom to top curves): 22, 37, 47, 55, 95, 121 and 161 minutes. Dashed line: the spectrum for a hexane solution of $Au_{5\ nm}$ particles (~0.3 μM). The insert: a plot of the absorbance of the SP band (590 nm) *vs.* immersion time (the baseline is drawn by extending the absorbance at 1100 nm to the entire region), where the solid line represents a theoretical fit of the data based on eqn. 5.

the SP band increases with increasing immersion time and levels off at ~200 min, which is shown by the inserted plot of absorbance *vs.* immersion time in Fig. 1. This trend is accompanied by a growth of the film thickness, as evidenced by the darkening of the bluish color of the film. The absorbance change serves as a qualitative indicator of the film growth.

Experiments using different concentrations of the nanoparticles and the linkers showed a similar trend. The formation rate is dependent on the concentration and ratio as well as the particle core size. For example, UV-Vis spectra of samples deposited on a number of glass slides that were taken at different immersion times from a diluted solution (0.13 μM $Au_{5\ nm}$ and 0.04 mM NDT) showed a slower increase of the SP absorbance and a leveling-off time at ~1300 minutes.

As stated, the lack of a distinctive SP band in the UV-Vis for $Au_{2\ nm}$ particles did not allow a quantitative assessment for the films derived from $Au_{2\ nm}$. Qualitatively, however, the overall rise in the UV-Vis absorbance in the SP band region with immersion time is consistent with the data for films derived from $Au_{5\ nm}$ particles. The thin film growth rate was much slower than that for the NDT–$Au_{5\ nm}$ film, even at higher concentrations of the nanoparticles.

Similar UV-Vis spectral dependences on immersion time were observed for the formation of MUA–$Au_{5\ nm}$ films. Fig. 2 presents a set of UV-Vis spectra for the formation of a MUA–$Au_{5\ nm}$ film from a hexane solution of 0.05 mM MUA and 1.0 μM $Au_{5\ nm}$. Again, the SP band showed evolutions in both wavelength and absorbance, with a subtle shift (from 575 nm to 590 nm) from its solution counterpart. This reflects a reduction of the interparticle distances to less than the particle sizes by the MUA-based linkages. The absorbance increases with increasing immersion time, as shown by the inserted plot in Fig. 2.

Both the concentration (nanoparticle or thiol) and the particle core size were found to affect the film formation rate. UV-Vis spectra for MUA–$Au_{5\ nm}$ films deposited on a number of glass slides at different immersion times from a diluted nanoparticle solution showed a much slower growth rate. When the nanoparticle concentration was too high, powder

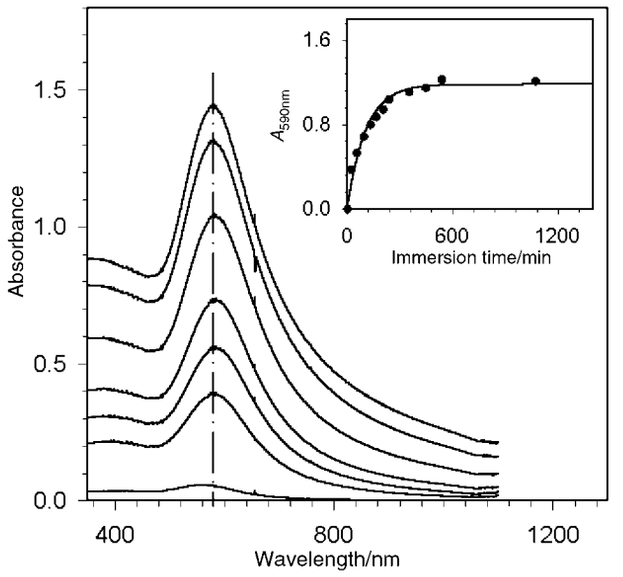

Fig. 2 UV-Vis spectra as a function of immersion time for the formation of MUA–$Au_{5\ nm}$ film from a hexane solution containing 1.0 μM $Au_{5\ nm}$ and 0.05 mM MUA. Immersion time increases from the bottom to the top. The immersion times are (from bottom to top curves): 22, 53, 94, 131, 237, 447 and 537 minutes. The insert: a plot of the absorbance of the SP band (590 nm) *vs.* immersion time, where the solid line represents a theoretical fit of the data based on eqn. 3.

precipitation was apparent, likely due to fast crosslinking or significant core–core aggregation of the particles during the exchange–crosslinking–precipitation process. For MUA–$Au_{2\ nm}$ particles, UV-Vis spectra were also similar to the data for NDT–$Au_{2\ nm}$ films in terms of the overall evolution in absorbance.

2. QCM mass-loading measurement

In the QCM measurement, the frequency change (Δf), which is proportional to the mass loading of the deposited nanoparticle film, was determined as a function of immersion time. Fig. 3 shows a set of the frequency change data for the formation of the NDT-linked particles of two different core sizes, *i.e.*, NDT–$Au_{5\ nm}$ (A) and NDT–$Au_{2\ nm}$ (B). For $Au_{5\ nm}$ (Fig. 3A), the solution contained 14 mM NDT and 1.8 μM $Au_{5\ nm}$. Clearly, Δf increases with the immersion time, indicating an increase of the thin film thickness. Qualitatively, the trend of the QCM data is comparable with the UV-Vis data for the same thin film formation process. The trend is also confirmed by experiments using multiple QCM devices for different immersion times or different concentrations of the nanoparticles and linkers. The rate of frequency change increases with increasing nanoparticle concentration.

For the smaller particle core size, $Au_{2\ nm}$ (Fig. 3B), QCM data revealed a similar trend in frequency change *vs.* immersion time in comparison with the data for NDT–$Au_{5\ nm}$ film. A difference in rate is however evident between the two core sizes, as reflected by the large difference of time length reaching the plateau. The formation of a NDT–$Au_{2\ nm}$ film (Fig. 3B) also requires a much higher nanoparticle concentration, *i.e.*, 14 mM NDT and 27 μM $Au_{2\ nm}$, for producing a significant frequency change in a limited timeframe.

For MUA-based nanoparticle films, we have observed interesting kinetic differences and similarities depending on the particle core sizes (Fig. 4), in comparison with the data for NDT-based films. Fig. 4A shows the frequency change as a function of immersion time for the formation of MUA–$Au_{5\ nm}$ from a solution of $Au_{5\ nm}$ particles (1.0 μM) and MUA (0.05 mM). The frequency change increases with increasing immersion time, indicative of the film thickness increase. The trend shows a subtle difference in comparison with the trend for the NDT–$Au_{5\ nm}$ film in terms of the curve shape.

Data obtained for the formation of MUA–$Au_{2\ nm}$ films (Fig. 4B), however, showed a curve shape similar to the previous NDT-based films. In addition, the formation of the MUA–$Au_{2\ nm}$ films was much slower than MUA–$Au_{5\ nm}$ films. The concentrations in the solution, *i.e.*, $Au_{5\ nm}$ (8.0 μM) and MUA (0.4 mM), needed to be much larger than that for the formation of the MUA–$Au_{5\ nm}$ films in order to observe a significant frequency change within a limited timeframe.

Overall, both QCM and UV-Vis data have shown that the nanoparticle film growth can be directly monitored by measuring the SP absorbance and mass loading as a function of immersion time. The results are strongly dependent on

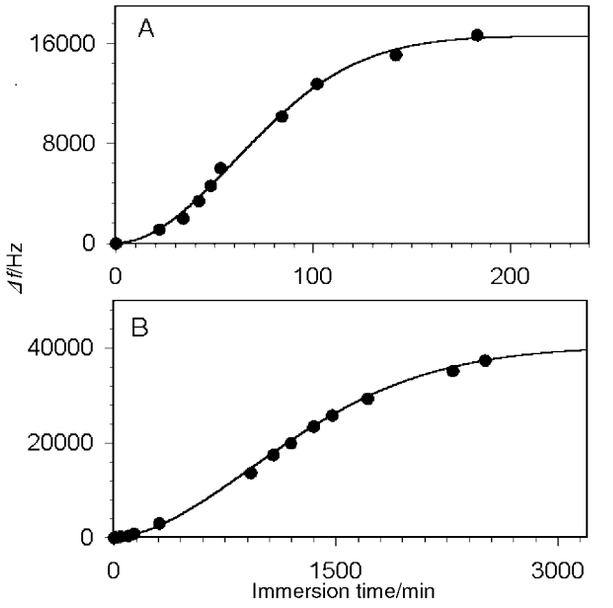

Fig. 3 Frequency decrease (Δf) of QCM as a function of immersion time for the film formation of (A) NDT–$Au_{5\ nm}$ and (B) NDT–$Au_{2\ nm}$, where the solid lines represent theoretically-fitted curves based on eqn. 5.

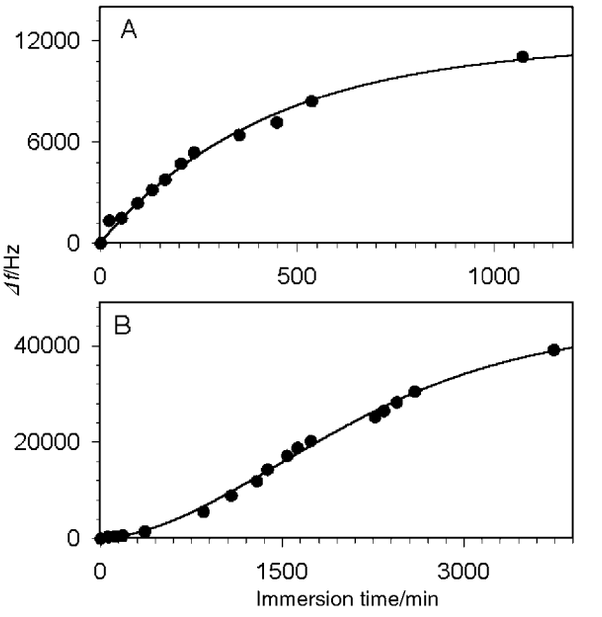

Fig. 4 Frequency decrease (Δf) of QCM as a function of immersion time for the film formation of (A) MUA–$Au_{5\ nm}$ and (B) MUA–$Au_{2\ nm}$, where the solid lines represent theoretically-fitted curves based on eqn. 3 (for A) and eqn. 5 (for B).

particle core sizes and concentrations of nanoparticles and linkers.

Discussion

Qualitatively, the evolution of the SP band provides information on the individual and collective properties of nanoparticles in the film, because its intensity and wavelength was known to be dependent on particle concentration, size, spacing, and medium.[15] Quantitatively, if all nanoparticles in the thin film are completely isolated by the thiol linkages and the SP band is independent of the packing properties, the absorbance may be related to the surface coverage of the assembled particles by, *e.g.*, absorbance (A) $\propto$ surface coverage of particles (Γ) or film thickness. Such a quantitative assessment is however complicated not only by the dependence on the medium or structural packing, but also by the poor-defined baseline of the UV-Vis spectra, particularly for thicker films. The frequency change of the QCM, on the other hand, provides an effective means to quantitatively correlate mass loading or film thickness with surface coverage. The resonance frequency, Δf, is related to mass change, Δm, according to the Sauerbrey equation[16]

$$\Delta m = -C_f \Delta f \quad (1)$$

where C_f is the sensitivity factor (5.7 ng cm^{-2} Hz for 9 MHz fundamental mode). This correlation is valid as long as it deals with a simple mass loading (*i.e.*, no viscoelastic effects) in less than 2% of the total weight of the crystal device,[16b] which is considered to be applicable for the thin films studied here.

Consider first the general similarities and differences between the inter-core reactivity for NDT–Au_{nm} and the inter-shell reactivity for MUA–Au_{nm}. According to Scheme 1, the initial exchange reactions between capping DT and solution MUA or NDT should be largely similar, though the rate and degree of exchange could be different. Place-exchange reaction of capped nanoparticles was recently shown by Murray and co-workers to be an initially rapid reaction that follows a first order associative pathway.[3b] It is thus reasonable to consider the follow-up crosslinking or exchange reactions as the initial stages of the film formation, *e.g.*, dimerization or nucleation. Differences in reaction kinetics between the two types of reactivity could affect the nucleation and growth kinetics of the linked "oligomers".

To a first approximation, we assume that the initial exchange is relatively fast and the follow-up crosslinking towards dimer or x-mers is a rate-determining step. The assumption is appropriate in view of the fact that in most cases the $HSC_{10}COOH$ or HSC_9SH component is in excess. If we further assume that the reaction is irreversible, the reaction rate in the solution can be expressed as

$$\frac{dC_{NP}}{dt} = -kC_{NP} \quad (2)$$

where C_{NP} is the concentration at time t, and k is the rate constant. This rate equation is valid under two extreme conditions: 1) particle deposition being the rate-determining step, and 2) particle deposition being diffusion controlled. Since the coverage of the deposited nanoparticles, $\Gamma_{NP\ film}$, can be considered to be proportional to concentration change, *i.e.*, ($C_{NP}{}^0$–C_{NP}), we have

$$\Gamma_{NP\,film} = -K(C_{NP}^0 - C_{NP}) = K'(1 - e^{-kt}) \quad (3)$$

where $C_{NP}{}^0$ is the initial concentration of the nanoparticles and K' is a constant. Eqn. 3 exhibits a simple exponential-rising character for the thin film growth.

Eqn. 3 is examined to see if it fits the experimental kinetic data, assuming both the SP absorbance and the QCM frequency change are proportional to the nanoparticle surface coverage, *i.e.*, Δf or $\Delta m \propto \Gamma_{NP\ film}$. Interestingly, it can fit reasonably well with the exponential-rising trend of both UV-Vis and QCM data for the MUA–$Au_{5\ nm}$ film, as shown by the solid lines in the UV-Vis data (Fig. 2 insert) and the QCM data (Fig. 4A). The fitted k parameters (Table 1) for the UV-Vis absorbance data and those for the QCM data differ by a factor of $\sim$4. The results are qualitatively consistent between the two very different measurements. Quantitatively, there is a significant difference in terms of the time scale for thin film growth. This difference can be better viewed by plotting the absorbance and mass change *vs.* time in the same graph (Fig. 5). Clearly, while the two sets of data are comparable for thinner films (*i.e.*, immersion time $<$ 200 min), the time length for leveling-off of the mass change (a, $>$1500 min) is greater than that for the absorbance data (b, $>$500 min).

Although eqn. 3 fits well with the data for the MUA–$Au_{5\ nm}$ film, it does not fit with the S- or sigmoidal-like trend for the other films studied, including NDT–$Au_{5\ nm}$, NDT–$Au_{2\ nm}$ and MUA–$Au_{2\ nm}$ films. A major reason is the oversimplification of the formation kinetics in the above considerations by the ignorance of a number of possible controlling factors in the overall thin film formation process such as core–shell exchange reactivity, diffusion, nucleation and growth. Since the above data were obtained under natural convection, an examination of the solution stirring effect should provide useful information on diffusion effects. Such an experiment is in fact demonstrated by QCM measurement of the thin film formation under solution stirring conditions. The result revealed that the film formation rate was much faster than that without stirring (by a factor of 2–5), as expected for a diffusion-controlled process. Clearly, the fit of eqn. 3 to the data supports a diffusion-controlled process for the formation of a MUA–$Au_{5\ nm}$ film. However, the failure to fit the rest of the data suggests that other factors may be operative in the overall kinetics. Further considerations of both diffusion and crystallization effects are needed for a more general assessment of the reactivities and kinetics.

It is known from early studies of crystallization kinetics of macromolecules or polymers[17,18] that the kinetic dependence of volume fractional crystallinity ($v(t)$) can be fitted to the modified treatment of Avrami's theoretical model for crystallization and growth,[19] which is generally expressed as

$$v(t) = 1 - e^{-kt^n} \quad (4)$$

where k is the rate constant and n is the critical growth exponent. This theoretical treatment has been used to describe crystallization kinetics of amorphous phases and to account for nucleation and growth kinetics.[17,18] Under conditions of diffusion-controlled mass flow to the crystal nucleus, a critical exponent of 2.5 or less has been observed for thermal

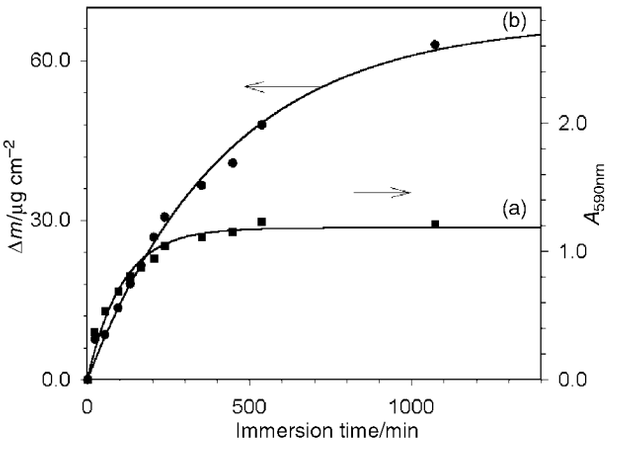

Fig. 5 A comparison of the UV-Vis absorbance (a) and QCM mass change (b) data for MUA–$Au_{5\ nm}$ films, where the solid lines represent theoretically-fitted curves based on eqn. 3.

Table 1 Summary of the fitting parameters based on eqn. 3 and 5

	QCM		UV-Vis	
Film	k	n	k	n
a) NDT–$Au_{5\ nm}$	1.6×10^{-4}	2.0	3.4×10^{-4}	2.0
b) NDT–$Au_{2\ nm}$	2.5×10^{-6}	1.8	—	—
c) MUA–$Au_{5\ nm}$	2.3×10^{-3}	1.0	9.3×10^{-3}	1.0
d) MUA–$Au_{2\ nm}$	1.0×10^{-6}	1.8	—	—

[a]Note: The fittings, a–d, were for the data in Fig. 1–4. Data for c were fitted by eqn. 3, and those for a, b and d were fitted by eqn. 5.

nucleation.[17] In an analogy to the above treatment, we may relate the formation of our thin films to a similar crystallization process involving nucleation and growth. Eqn. 4 is re-written as

$$\Gamma_{\mathrm{NPfilm}} = K(1-\mathrm{e}^{-kt^n})$$

where the surface coverage ($\Gamma_{\mathrm{NP\ film}}$) is considered to be proportional to the volume fractional crystallinity ($v(t)$) in the film.

Eqn. 5 fits the experimental sigmodial-like UV-Vis and QCM data surprisingly well, as shown by the solid lines in Fig. 1, 3 and 4B. The fitted n values in each case are very close to 2 (Table 1), suggestive of a mechanism involving a thermal nucleation and three-dimensional crystallization, as often found for macromolecule systems.[17,18] The previous fit of eqn. 3 to the MUA–$Au_{5\ nm}$ data (Fig. 5) can be considered as a special case of this model where $n=1$. Smaller values of n were considered as indications of lower growth dimensionality.[17] The fitted k values (Table 1), on the other hand, provide important parameters for assessing the growth rate. For NDT–$Au_{5\ nm}$ film, the k values for the absorbance and the frequency change data differ only by a factor of $\sim$2. The formation rate for the NDT–$Au_{5\ nm}$ is greater than that for the NDT–$Au_{2\ nm}$ film (by $\sim$2 orders of magnitude). The rate constant from the QCM data of MUA–$Au_{2\ nm}$ is also much smaller than that for the MUA–$Au_{5\ nm}$ (Table 1). The particle core size thus constitutes an important factor in determining the film growth rate.

Fig. 6 shows a comparison of UV-Vis and QCM kinetic data for the NDT–$Au_{5\ nm}$ film, in which Δf is converted to Δm. Conclusions similar to the case for MUA–$Au_{5\ nm}$ film formation (Fig. 5) can be reached. In general, the UV-Vis absorbance data and the QCM data are comparable in the early stages of the film formation (*i.e.*, immersion time $<$100 min). As the film grows thicker, the absorbance data reach a plateau earlier (a, $\sim$100 min) than the QCM data (b, $\sim$200 min). The plateau feature is a consequence of the ultimate depletion of nanoparticles in the bulk solution, as evidenced by two observations. In the first, the colored solution was found to become clear after a period of reaction time (a few hours to days depending on concentrations and compositions). Secondly, our UV-Vis experiments have indicated that both the solution nanoparticles and the thin film nanoparticles formed after the solution became clear showed a linear relationship to the concentration of the starting nanoparticles in the solution. The difference between UV-Vis and QCM data is believed to be due to packing evolution or annealing effects during film growth, which may affect the SP resonance band *via* changes in interparticle electronic and medium properties.

Based on the QCM data, we further estimated the equivalent number of particle layers in the film. By assuming a dense (111)-type packing of spherical particles[20] on a planar surface with either NDT linkages (interparticle distance $\sim$1.5 nm) or head-to-head hydrogen-bonded MUA linkages (interparticle distance $\sim$3.6 nm), one equivalent layer would correspond to 2.2 (MUA–$Au_{5\ nm}$), 0.37 (MUA–$Au_{5\ nm}$), 4.0 (NDT–$Au_{5\ nm}$) or 0.92 μg cm^{-2} (NDT–$Au_{5\ nm}$). Based on these estimates, one

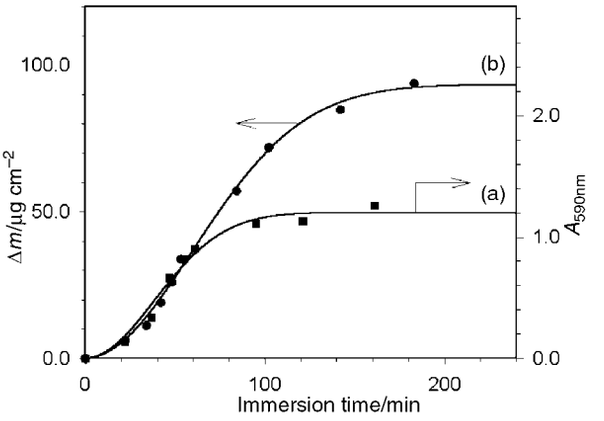

Fig. 6 A comparison of the UV-Vis absorbance (a) and QCM mass change (b) data for NDT–$Au_{5\ nm}$ films, where the solid lines represent theoretically-fitted curves based on eqn. 5.

concludes that both UV-Vis and QCM data provide a comparable assessment of the kinetic process for $\sim$10 layers of the initial MUA–$Au_{5\ nm}$ or NDT–$Au_{5\ nm}$ films. As the film grows thicker (up to 30–100 layers), other factors such as packing evolution or annealing may be operative due to particle spacing and medium effects.

Several factors governing the nanoparticle thin film formation and growth processes emerge from the above analyses of the experimental data. First, the identity of binding sites at the core–shell nanoparticles plays an important role in the formation of the nanoparticle films. The difference between the initially slow sigmoidal-type growth of NDT–$Au_{5\ nm}$ films and the initially fast exponential growth of MUA–$Au_{5\ nm}$ films supports this assessment. This difference may be accounted for by a lower cost of activation energy of the shell–shell reactivity for the MUA–$Au_{5\ nm}$ film, in comparison with a large energy cost for the core–shell reactivity (Au–S bonding) for NDT–$Au_{5\ nm}$ films. In addition, the hydrophilic character of the –COOH group of MUA may be another factor that energetically facilitates the hydrogen-bonding reactivity. Overall, the structural differences between the two functionalized thiols are closely related to their reaction differences in terms of the inter-shell and the inter-core linking reactivities.

Secondly, the core size was shown to play an important role in the film formation process. The difference in film growth rate between $Au_{5\ nm}$ and $Au_{2\ nm}$ may suggest that the exchange is less favored for the more densely packed thiolate monolayers on $Au_{2\ nm}$ than that on $Au_{5\ nm}$ cores. The $Au_{5\ nm}$ particles are known to be highly faceted with more defects in the encapsulation layer than on $Au_{2\ nm}$ due to increased crystal corner or edge effects.[1,14] The assessment is further supported by recent results of place-exchange reactions of thiolate-capped Au nanoparticles[3b] which demonstrated that place-exchange at defect sites or crystal edges or corners was more favorable than on terrace sites.

Thirdly, an annealing process associated with structural packing of the particles may be operative as the film grows thicker. This may be reflected by the discrepancy between the UV-Vis and the QCM kinetic data for films thicker than $\sim$10 equivalent layers. Two additional sets of preliminary data further support the assessment. First, the noticeable red shift of the SP band as a function of immersion time may reflect a more cohesive interaction and dense packing of the particles. Secondly, the evolution of methylene stretching bands (2920 and 2850 cm^{-1}) observed in IRS data towards lower wavenumber with increasing immersion time (5–10 cm^{-1} [11–12]) may be considered as an indicator of highly crystalline alkyl chain packing, as is known for both self-assembled monolayers on planar gold substrates and on gold nanoparticles.[21–22]

The above kinetic assessment of the nanoparticle film

formation and growth has important implications for designing and fabricating nanostructured materials using core–shell nanoparticles as building blocks for molecular recognition and catalysis. These applications often require the ability to control thickness, molecular packing, nanocrystal isolation, or size-specific porosity. Knowledge of the inter-core or inter-shell reactivities and their dependences on particle core size and molecular linker structure can provide valuable guidance for developing these abilities.

Conclusion

In conclusion, we have shown that both UV-Vis and QCM measurements provide useful kinetic information for assessing the inter-core and inter-shell molecular reactivities in the formation and growth of molecularly-linked core–shell nanoparticle thin films. The evolution of the surface plasmon resonance band in absorbance and wavelength relates qualitatively to both the individual property of shell- or linker-isolated particle cores and the collective properties of particles in the network films. The mass loading data provide a quantitative correlation of the surface coverage with the film growth. It is important to point out that the difference in substrates between the QCM and the UV-Vis studies is likely to have an impact on the effective thickness of the films. A direct correlation between the two sets of data could thus be complicated. A further examination of the film morphologies at different film growth stages using transmission electron microscopic and atomic force microscopic techniques is underway to provide an in-depth assessment of the thin film growth processes.

We believe that the identity of binding or linking sites constitutes an important controlling factor. The inter-shell reactivity is shown to be more effective than the inter-core reactivity, which is qualitatively consistent with energetic and steric considerations of the binding sites. We also conclude that the core size of nanoparticles constitutes an important factor in the overall reactivity. Exchange and crosslinking at the 5 nm particles are more effective than those at the 2 nm particles, which may be attributed to the fact that the packing density on the larger-sized particles is smaller than that on the smaller-sized particles. Packing defects at the highly faceted crystals[3b,14] are likely the binding sites for effective exchange or crosslinking. In comparison with core–shell nanoparticles derived from inorganic cores capped by inorganic shells (*e.g.* CdSe/CdS),[23] the organic shell encapsulation for our nanoparticle system provides a platform for versatile interfacial manipulation *via* shell functional groups. A detailed delineation of the interfacial structures with the design of molecular recognition and catalytic nanomaterials in terms of core–shell reactivities and sizes is the subject of future reports.

Acknowledgements

The ACS Petroleum Research Fund is acknowledged for support of this research.

References

1 A. C. Templeton and R. W. Murray, *Acc. Chem. Res.*, 2000, **33**, 27, and references therein.
2 C. J. Kiely, J. Fink, M. Brust, D. Bethell and D. J. Schiffrin, *Nature*, 1998, **396**, 444.
3 (*a*) M. J. Hostetler, S. J. Green, J. J. Stokes and R. W. Murray, *J. Am. Chem. Soc.*, 1996, **118**, 4212; (*b*) M. J. Hostetler, C. Templeton and R. W. Murray, *Langmuir*, 1999, **15**, 3782.
4 (*a*) C. S. Weisbecker, M. V. Merritt and G. M. Whitesides, *Langmuir*, 1996, **12**, 3763; (*b*) S. R. Johnson, S. D. Evans and R. Brydson, *Langmuir*, 1998, **14**, 6639.
5 (*a*) J. Fink, C. J. Kiely, D. Bethell and D. J. Schiffrin, *Chem. Mater.*, 1998, **10**, 922; (*b*) R. L. Whetten, J. T. Khoury, M. M. Alvarez, S. Murthy, L. Vezmar, Z. L. Wang, P. W. Stephens, C. L. Cleveland, W. D. Luedtke and U. Landman, *Adv. Mater.*, 1996, **8**, 428; (*c*) Z. L. Wang, J. M. Petroski, T. C. Green and M. A. El-Sayed, *J. Phys. Chem. B*, 1998, **102**, 6145; (*d*) R. H. Terrill, T. A. Postlethwaite, C. H. Chen, C. D. Poon, A. Terzis, A. D. Chen, J. E. Hutchison, M. R. Clark, G. Wignall, J. D. Londono, R. Superfine, M. Falvo, C. S. Johnson, E. T. Samulski and R. W. Murray, *J. Am. Chem. Soc.*, 1995, **117**, 12537.
6 (*a*) M. Brust, D. Bethell C. J. Kiely and D. J. Schiffrin, *Langmuir*, 1998, **14**, 5425; (*b*) M. Brust, D. Bethell, D. J. Schiffrin and C. J. Kiely, *Adv. Mater.*, 1995, **7**, 795.
7 (*a*) R. P. Andres, J. D. Bielefeld, J. I. Henderson, D. B. Janes, V. R. Kolagunta, C. P. Kubiak, W. J. Mahoney and R. G. Osifchin, *Science*, 1996, **273**, 1690; (*b*) M. D. Musick, D. J. Pena, S. L. Botsko, T. M. McEvoy, J. N. Richardson and M. J. Natan, *Langmuir*, 1999, **15**, 844; (*c*) J. H. Fendler, *Chem. Mater.*, 1996, **8**, 1616.
8 (*a*) K. Hu, M. Brust and A. J. Bard, *Chem. Mater.*, 1998, **10**, 1160; (*b*) C. Demaille, M. Brust, M. Tsionsky and A. J. Bard, *Anal. Chem.*, 1997, **69**, 2323.
9 (*a*) R. Elghanian, J. J. Storhoff, R. C. Mucic, R. L. Letsinger and C. A. Mirkin, *Science*, 1997, **277**, 1078; (*b*) R. C. Mucic, J. J. Storhoff, C. A. Mirkin and R. L. Letsinger, *J. Am. Chem. Soc.*, 1998, **120**, 12674.
10 D. Bethell, M. Brust, D. J. Schiffrin and C. J. Kiely, *J. Electroanal. Chem.*, 1996, **409**, 137.
11 W. X. Zheng, M. M. Maye and C. J. Zhong, *Anal. Chem.*, 1999, **71**, 5076.
12 (*a*) W. X. Zheng, M. M. Maye, F. L. Leibowitz and C. J. Zhong, *Analyst*, 2000, **125**, 17; (*b*) W. X. Zheng, M. M. Maye, F. L. Leibowitz and C. J. Zhong, *Anal. Chem.*, 2000, **72**, 2190.
13 (*a*) M. Brust, M. Walker, D. Bethell, D. J. Schiffrin and R. Whyman, *J. Chem. Soc., Chem. Commun.*, 1994, 801; (*b*) M. Brust, J. Fink, D. Bethell, D. J. Schiffrin and C. J. Kiely, *J. Chem. Soc., Chem. Commun.*, 1995, 1655; (*c*) M. J. Hoetetler, J. E. Wingate, C. J. Zhong, J. E. Harris, R. W. Vachet, M. R. Clark, J. D. Londono, S. J. Green, J. J. Stokes, G. D. Wignall, G. L. Glish, M. D. Porter, N. D. Evans and R. W. Murray, *Langmuir*, 1998, **14**, 17.
14 (*a*) M. M. Maye, W. X. Zheng, F. L. Leibowitz, N. K. Ly and C. J. Zhong, *Langmuir*, 2000, **16**, 490; (*b*) M. M. Maye and C. J. Zhong, *J. Mater. Chem.*, 2000, **10**, 1895.
15 M. M. Alvarez, J. T. Khoury, T. G. Schaaff, M. N. Shafigullin, I. Vezmar and R. L Whetten, *J. Phys. Chem. B*, 1997, **101**, 3706.
16 (*a*) D. A. Buttry and M. D. Ward, *Chem. Rev.*, 1992, **92**, 1355; (*b*) *Applications of Piezoelectric Quartz Crystal Microbalances*, ed. C. Lu and A. W. Canderna, Elsevier, Amsterdam, 1984.
17 G. J. Exarhos and M. Aloi, *Thin Solid Films*, 1990, **193**, 42.
18 S. Z. D. Cheng and B. Wunderlich, *Macromolecules*, 1988, **21**, 3327.
19 M. Avrami, *J. Chem. Phys.*, 1940, **8**, 212.
20 The number of Au atoms, N_{Au}, and of thiolates, N_{RS}, are calculated by $N_{Au}=(4/3)\pi R^3/V_g$ and $N_{RS}=4\pi R^2/A_{RS}$, in which R, V_g, and A_{RS} are core radius, core density and thiolate density, respectively. The estimate yields $\sim$3850 Au atoms and $\sim$370 dithiolates for the 5 nm particle and $\sim$250 Au atoms and $\sim$60 dithiolates for the 2 nm particle.
21 M. J. Hostetler, J. J. Stokes and R. W. Murray, *Langmuir*, 1996, **12**, 3604.
22 M. J. Hostetler and R. W. Murray, *J. Curr. Opin. Colloid Interface Sci.*, 1997, **2**, 42, and references therein.
23 (*a*) X. Peng, M. C. Schlamp, A. V. Kadavanich and A. P. Alivisatos, *J. Am. Chem. Soc.*, 1997, **119**, 7019; (*b*) H. Mattoussi, J. M. Mauro, E. R. Goldman, G. P. Anderson, V. C. Sundar, F. V. Mikulec and M. G. Bawendi, *J. Am. Chem. Soc.*, 2000, **122**, 12142.